MEDDOCS Open Access Publisher

Nanoscience and Nanotechnology: Open Access

Open Access | Mini Review

Recent Progress of Cation-Disordered Rock-Salt Cathode Materials for Next-Generation Cobalt-Free Lithium-Ion Batteries

Peiyuan Guan[1]*; Bohan Hao[1]; Yiming Xia[1]; Hao Wang[1]; Zhemi Xu[2]

[1]School of Materials Science and Engineering, University of New South Wales, Sydney, 2052, Australia.

[2]Chemistry and Material Engineering College, Beijing Technology and Business University, Beijing 100048, China.

Corresponding Author(s): Peiyuan Guan

School of Materials Science and Engineering, University of New South Wales, Sydney, 2052, Australia.

Email: peiyuan.guan@unsw.edu.au

Received: Nov 29, 2022

Accepted: Dec 29, 2022

Published Online: Dec 31, 2022

Journal: Nanoscience and Nanotechnology: Open Access

Publisher: MedDocs Publishers LLC

Online edition: http://meddocsonline.org/

Keywords: Lithium-ion batteries; Cation-disordered rock-salt oxides; Cobalt-free cathode materials; Electrochemical properties; Improvement strategies.

Abstract

Cathode, a key component in lithium-ion batteries (LIBs), has received substantial attention since the first LIB emerged in the 1990s. Currently, cobalt-based cathodes are dominant in commercial LIBs, not only leading to a tight supply of cobalt resources but also exerting potential risk on battery recycling. To alleviate these situations, cation-disordered rock-salt (CDRS) cathodes containing no cobalt have been intensively investigated in recent years because of their high energy density originating from cumulative cationic and anionic redox activities. In this work, we initially reviewed prevalent CDRS cathode materials, including their structures and electrochemical properties. Afterwards, a summarization of the most updated research progress on the improvement strategies for CDRS cathodes is provided. Finally, the challenges faced, and future guidelines for optimizing CDRS cathode materials are discussed. This mini-review may shed light on the further development of CDRS-type oxides in the next generation of cobalt-free LIBs.

Background and Motivation

Lithium-Ion Battery (LIB) is one of the most successful commercial secondary batteries in the 21st century due to its high operation potential and large specific capacity. To date, LIBs are regarded as a dominant power source for portable electronics. They can even be integrated into electric vehicles (EVs) to relieve environmental issues triggered by internal combustion engine vehicles (ICEVs) [1]. Among the four main components of a LIB (i.e., cathode, anode, electrolyte and separator), the cathode is the most critical part because it serves as the primary lithium-ion (Li^+) donor for the electrochemical reaction. In addition, the cathode occupies the highest proportion (≥ 30%) in a LIB cell. Therefore, cathode properties materials significantly affect the electrochemical performance and cost of LIBs [2].

At present, cobalt (Co)-contained cathodes possessed high percentages in commercialized high-energy LIBs, such as $LiCoO_2$ (LCO) [3], $LiNi_xCo_yMn_{1-x-y}O_2$ (NCM) [4], and $LiNi_xCo_yAl_{1-x-y}O_2$ (NCA) [5]. However, the commercial success of these Co-containing cathodes induces supply shortages and price increases of Co raw materials, which severely swing the cost of LIBs. Furthermore, Co is toxic for miners and also raises the potential risk for recycling LIBs. Therefore, new types of cathodes are urgently needed to overcome these obstacles and further increase output power for Co-free LIBs in terms of material level [6].

Cite this article: Guan P, Zhemi Xu, Bohan H, Xia Y, Wang H. Recent Progress of Cation-Disordered Rock-Salt Cathode Materials for Next-Generation Cobalt-Free Lithium-Ion Batteries Nanosci Nanotechnol Open Access. 2022; 1(1): 1007.

Recently, Cation-Disordered Rock-Salt (CDRS) oxides ($Li_{1+x}M_yM'_{1-x-y}O_2$, M=Ti, V, Zr, Nb, Mo, etc. and M'= Mn, Fe, Ni etc.) have attracted increasing research interests because they demonstrate promising features to be one of the alternatives for the next-generation Co-free LIBs that can be employed in portable devices and EV markets. First, CDRS cathodes can provide higher energy densities than conventional cathode materials benefiting from their excess Li content in the crystal structure. Besides, both cations and anions in the crystalline of CDRS material can participate in electrochemical redox under the applied voltage range [7]. Second, these kind of oxide can sustain a longer lifespan attributed to their robust structures, which experience minorer volumic variations during charge and discharge cycles. Third, because of the unique composition of CDRS materials, expansive and toxic Co content can be eliminated from their structure without compromising the electrochemical performances. Hence, reviewing current research progress on Co-free CDRS cathodes is timely and necessary.

In this work, we summarise the recent CDRS materials-based cathode development for LIBs. Firstly, an overview of Co-free CDRS oxides is presented to classify the differences from the traditional intensively studied cathode materials. Furthermore, trendy research based on CDRS cathodes is investigated and concluded, among which outstanding works are selected to disclose the relationships between structures and electrochemical performances. At last, modification strategies for current CDRS materials are reviewed, and future conceptions are proposed based on the state-of-art research achievements.

Overview of Cation-Disordered Rock-Salt Cathode Materials

The first proposal of Li-contained CDRS oxide can trace back to 1990, Castellanos et al. reported a series of compounds with α-$LiFeO_2$ structure: Li_2MXO_4 (M=Zr and Hf; X=Mg, Mn, Fe, Co, Ni, Cu, and Zn), in particular, M and X ions are disordered over the octahedral Fe sites [8]. However, following research found that a random distribution of Li exists in this structure, which hinders Li^+ internal diffusions, so CDRS oxide had been slighted alongside the successful commercialization of LCO in the early 2000s [9]. Since the first fully LIB-powered EV (Roadster: first generation) was released by Tesla in 2008, more attention has been attracted to cathode modifications to approach lower cost and higher energy density. Under this trend, people gradually realized that multielement layered structure Transition Metal (TM) oxides exhibited promising potential as cathodes for LIB that can be integrated into EVs. Within the deepening research, modified CDRS oxides derived from layered structure oxides returned to the scientific community's perspective [10]. A berife evolutionary path is demonstrated in **Figure 1.**

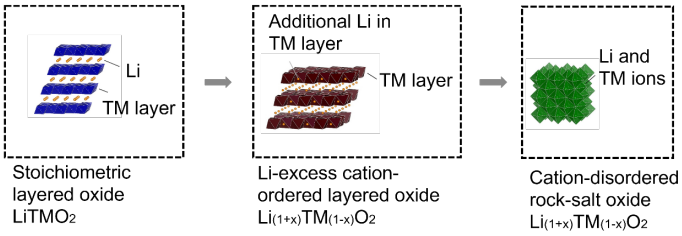

Figure 1: Evolutionary routes of cathode materials, from layered structure oxides to CRRS oxides. Re-designed with permission from ref. [11] © 2022 Elsevier B.V.

Generally, current available CDRS oxides are featured by percolative Li migration, termed 0-TM percolation [12]. Li^+, initially located at the octahedral sites, then migrate to neighbouring and vacant octahedral sites through intermediate tetrahedral sites. Weak repulsive interactions are favoured for Li^+ transmission only when the intermediate tetrahedral sites share faces with Li^+ and without TM ions (0-TM). In the Li-excess compositions, the probability of percolative Li migration through 0-TM channels increases, inducing facile Li transportation in CDRS oxides [9]. Therefore, the most investigated CDRS cathode materials nowadays share a generic format with Li-rich layered oxides: $Li_{(1+x)}TM_{(1-x)}O_2$. However, the TM element candidates that can be integrated into CDRS oxides are broader than those of Li-rich cathodes.

Table 1: Summary of CDRS cathode materials and their electrochemical performances.

Element composition	Chemical formula	Voltage	Initial discharge capacities (current density)	Capacity retention (cycles)	High-rate or different temperature testing	Ref.
Li-Mn-Ti-O	$LiMn_{0.5}Ti_{0.5}O_2$	2.0-4.7 V	145 mAh/g (7.5 mA/g)	86% (15)	At 58 mA/g, $Li_{1.2}Mn_{0.4}Ti_{0.4}O_2$ delivered 184 mAh/g with a capacity retention of 78%.	[13]
	$Li_{1.1}Mn_{0.45}Ti_{0.45}O_2$		163 mAh/g (7.5 mA/g)	90% (15)		
	$Li_{1.2}Mn_{0.4}Ti_{0.4}O_2$		226 mAh/g (7.5 mA/g)	82% (15)		
	$Li_{1.3}Mn_{0.35}Ti_{0.35}O_2$		184 mAh/g (7.5 mA/g)	79% (15)		
	$Li_{1.2}Mn_{0.4}Ti_{0.4}O_2$	1.5-4.8 V	> 300 mAh/g (5 mA/g)	> 85% (5)	Cycled at 50 ^{O}C	[14]
		1.1-1.7 V	~ 208 mAh/g (10 mA/g)	> 80% (10)	Under 50 ^{O}C, the initial discharge capacity increased 27% compared to that of cycled at room temperature. At 260 mA/g, it still delivered a discharge capacity of 150 mAh/g.	[15]
Li-Mn-Nb-O	$Li_{1.05}Mn_{0.9}Nb_{0.05}O_2$	1.5-4.8 V	~ 250 mAh/g (40 mA/g)	85% (40)	When cycled at 100 mA/g , $Li_{1.05}Mn_{0.9}Nb_{0.05}O_2$ and $Li_{1.2}Mn_{0.6}Nb_{0.2}O_2$ delivered a discharge capacity of 223 mAh/g and 260 mAh/g, respectively.	[16]
	$Li_{1.1}Mn_{0.8}Nb_{0.1}O_2$		~ 255 mAh/g (40 mA/g)	78% (35)		
	$Li_{1.2}Mn_{0.6}Nb_{0.2}O_2$		~ 277 mAh/g (40 mA/g)	69% (40)		
	$Li_{1.25}Mn_{0.5}Nb_{0.25}O_2$		249.9 mAh/g (10 mA/g)	75.8% (30)	-	[17]
	$Li_{1.2}Mn_{0.6}Nb_{0.2}O_2$		232 mAh/g (10 mA/g)	92.7% (20)	-	[18]
	$Li_{1.3}Mn_{0.4}Nb_{0.3}O_2$		271 mAh/g (10 mA/g)	60.9% (20)		
	$Li_{1.4}Mn_{0.2}Nb_{0.4}O_2$		268 mAh/g (10 mA/g)	49.6% (20)		

Li-Mn-Nb-O	$Li_{1.2}Mn_{0.6}Nb_{0.2}O_2$		255 mAh/g (20 mA/g)	60% (100)	At 400 mA/g, $Li_{1.2}Mn_{0.6}Nb_{0.2}O_2$ delivered 208 mAh/g.	[19]
	$Li_{1.3}Mn_{0.4}Nb_{0.3}O_2$		~ 290 mAh/g (10 mA/g)	~ 55% (27)	-	[20]
			~ 250 mAh/g (20 mA/g)	~ 32% (50)		[21]
		1.0-4.8 V	~ 300 mAh/g (10 mA/g)	~ 61% (20)	Cycled at 60 ^{O}C. At 1600 mA/g, it still delivered capacity higher than 160 mAh/g.	[22]
Li-Mn-Ta-O	$Li_{1.3}Mn_{0.4}Ta_{0.3}O_2$	1.5-4.8 V	~ 250 mAh/g (10 mA/g)	~ 30% (30)	-	[23]
		1.0-4.8 V	180 mAh/g (10 mA/g)	~ 64% (10)	Under 55 ^{O}C, the initial discharge capacity increased to 230 mAh/g	[24]
Li-Mn-Zr-O	$Li_{1.2}Mn_{0.4}Zr_{0.4}O_2$	1.5-4.7 V	~ 135 mAh/g (10 mA/g)	~ 55% (10)	Under 50 ^{O}C, the initial discharge capacity increased 53% compared to that of cycled at room temperature.	[15]
Li-Mn-Ni-Mo-O	$Li_{6/5}Mni_{1/5}Ni_{2/5}Mo_{1/5}O_2$	1.5-4.8 V	~ 200 mAh/g (10 mA/g)	~ 60% (30)	-	[25]
	$Li_{9/8}Mni_{5/16}Ni_{7/16}Mo_{1/8}O_2$		240 mAh/g (10 mA/g)	~ 75% (10)		
	$Li_{9/7}Mn_{1/14}Ni_{5/14}Mo_{2/7}O_2$		~ 130 mAh/g (10 mA/g)	-		
	$Li_{5/4}Mn_{1/18}Ni_{3/8}Mo_{1/4}O_2$		~ 170 mAh/g (10 mA/g)	-		
Li-Ni-Ti-O	$Li_{1.1}Ni_{0.35}Ti_{0.55}O_2$	2.5-4.5 V	116.5 mAh/g (40 mA/g)	85.8% (50)	At 400 mA/g, $Li_{1.1}Ni_{0.35}Ti_{0.55}O_2$ delivered more than 50 mAh/g.	[26]
	$Li_{1.17}Ni_{0.25}Ti_{0.58}O_2$	1.5-4.5 V	223.9 mAh/g (20 mA/g)	81.9% (50)	$Li_{1.17}Ni_{0.25}Ti_{0.58}O_2$ delivered about 120 mAh/g at 400 mA/g.	[27]
Li-Ni-Ti-Mo-O	$Li_{1.2}Ni_{1/3}Ti_{1/3}Mo_{2/15}O_2$		223 mAh/g (20 mA/g)	> 90% (10)	$Li_{1.2}Ni_{1/3}Ti_{1/3}Mo_{2/15}O_2$ delivered 120 mAh/g at 400 mA/g.	[28]
			~ 220 mAh/g (20 mA/g)	~ 62% (50)	$Li_{1.2}Ni_{1/3}Ti_{1/3}Mo_{2/15}O_2$ delivered 95 mAh/g at 400 mA/g.	[29]
		1.5-4.6 V	215 mAh/g (20 mA/g)	49% (100)	$Li_{1.2}Ni_{1/3}Ti_{1/3}Mo_{2/15}O_2$ delivered 120 mAh/g at 400 mA/g.	[19]
Li-Ni-Ti-Nb-O	$Li_{1.2}Ni_{0.3}Ti_{0.3}Nb_{0.2}O_2$	1.5-4.5 V	221.5 mAh/g (20 mA/g)	~ 80% (50)	$Li_{1.2}Ni_{0.3}Ti_{0.3}Nb_{0.2}O_2$ delivered 119.7 mAh/g at 400 mA/g.	[30]
Li-Ni-Nb-O	$Li_{1.2}Ni_{0.4}Nb_{0.4}O_2$	1.0-4.8 V	> 230 mAh/g (10 mA/g)	~ 72% (30)	Under 60 ^{O}C, the initial discharge capacity increased to 303 mAh/g compared to that of cycled at room temperature.	[31]
	$Li_{1.3}Ni_{0.27}Nb_{0.43}O_2$		~ 300 mAh/g (10 mA/g)	~ 17% (10)	Cycled at 60 ^{O}C.	[22]
	$Li_{1.8}Ni_{0.4}Nb_{0.6}O_{2.8}$	1.5-4.5 V	155.35 mAh/g (20 mA/g)	82.9% (40)	$Li_{1.8}Ni_{0.4}Nb_{0.6}O_{2.8}$ delivered 116 mAh/g at 1000 mA/g.	[32]
Li-Ni-Ta-O	$Li_{1.3}Ni_{0.27}Ta_{0.43}O_2$	1.0-4.8 V	~ 220 mAh/g (10 mA/g)	~ 80% (10)	Under 55 ^{O}C, the initial discharge capacity kept at ~220 mAh/g	[24]
Li-Ni-Sb-O	$Li_{1.15}Ni_{0.47}Sb_{0.38}O_2$	2.5-4.6 V	132 mAh/g (225 mA/g)	~ 80% (50)	-	[33]
Li-Ni-Ru-O	$Li_{1.23}Ni_{0.155}Ru_{0.615}O_2$	2.2 -4.3 V	295.3 mAh/g (25 mA/g)	~ 67.1% (50)	$Li_{1.8}Ni_{0.4}Nb_{0.6}O_{2.8}$ delivered about 150 mAh/g at 250 mA/g.	[34]
	$Li_2Ni_{1/3}Ru_{2/3}O_2$	2.0-4.3 V	227 mAh/g (20 mA/g)	94.2% (150)	$Li_2Ni_{1/3}Ru_{2/3}O_2$ delivered 84 mAh/g at 500 mA/g.	[35]
Li-Nb-V-O	$Li_{1.25}Nb_{0.25}V_{0.5}O_2$	1.5-4.8 V	227 mAh/g (10 mA/g)	~ 90% (100)	Under 50 ^{O}C, the initial discharge capacity increased to 300 mAh/g	[36]
	$Li_{1.3}Nb_{0.3}V_{0.4}O_2$		~ 230 mAh/g (10 mA/g)	~ 100% (50)	The reversible capacity increased from 160 to 210 mAh/g when cycleed at 60 °C (1.5-4.2 V).	[37]
			~ 200 mAh/g (5 mA/g)	> 80% (5)	Cycled at 50 ^{O}C	[14]
Li-Nb-Fe-O	$Li_{1.3}Nb_{0.3}Fe_{0.4}O_2$		~ 250 mAh/g (5 mA/g)	> 90% (5)		
			225.8 mAh/g (20 mA/g)	~ 45% (50)	-	[21]
Li-Nb-Mo-O	$Li_{9/7}Nb_{2/7}Mo_{3/7}O_2$	1.0-4.4 V	~ 280 mAh/g (10 mA/g)	~ 90% (30)	$Li_{9/7}Nb_{2/7}Mo_{3/7}O_2$ delivered about 250 mAh/g at 100 mA/g with a 90% capacity retention after 60 cycles.	[38]
Li-Mo-Ti-O	$Li_{6/5}Mo_{2/5}Ti_{2/5}O_2$		~ 280 mAh/g (10 mA/g)	~ 90% (30)	-	
Li-Mo-Cr-O	$Li_{1.211}Mo_{0.467}Cr_{0.322}O_2$	1.5-4.3 V	265.6 mAh/g (16.4 mA/g)	> 90% (10)		[9]

Table 1 classified and summarized Co-free Li-excess CDRS oxide-based cathodes and their electrochemical properties in the last decade. It can summarize that the CDRS oxides deliver higher specific capacities in most cases compared with conventional cathode materials with layered frameworks (~140 mAh/g). Moreover, TM selections are limited for layered structure oxides because they should be smaller than Li^+ (0.90 Å) to maintain a relatively stable structure. However, CDRS cathodes are benefited from the rock-salt host structures that endure more deformations during Li^+ intercalation/deintercalation [11]. Therefore, a broad of TM elements, even with higher oxidation states (e.g., Ti^{4+}, V^{5+}, Zr^{4+}, Nb^{5+}, Mo^{6+}, etc.), can be feasibly integrated into the crystal design for the CDRS cathodes. Urban et al. have noted that TM ions with no electron occupied d- orbital (d^0) in their electronic structure favoured to stabilize the CRDS structure owing to the tolerance to distortion formed by the different local environments with various cations [39].

Although the enhanced stability of CDRS oxides enlightened a new path for synthesising cathode materials, significant challenges for CDRS-based cathodes, such as severe capacity degradation during long cycles, are still impeding them be employed in commercial LIBs. Herein, the benefits and drawbacks of CDRS cathodes compared to currently commercialized cathodes are listed in Table 2. It indicated that CDRS cathode materials need to be further optimized to achieve long-term electrochemical reaction stabilities, which will detailed discuss in the next section.

Table 2: Comparison of advantages and disadvantages between CDRS cathodes and current commericalized layered structure cathodes.

	Advantages	Disadvantages	Ref.
CDRS cathodes	• Wider and cheaper available raw materials (toxic cobalt can be fully eliminated); • Li-excess contained (could provide higher energy densities due to more Li^+ reservoir); • Stable crystal structure and excellent high-temperature performance (High safety).	• Fast capacity degradation leading to short cyclic stability; • Poor rate performance induced by inferior electrochemical kinetics; • Limited Li^+ diffusion rate causing voltage hysteresis; • Low initial coulombic efficiency.	[12, 40, 41]
Layered cathodes	• Acceptable power output and lifespan; • Proven manufacturing procedures; • Intensively studied optimization strategies • Relatively simple redox process.	• Over-reliance on cobalt, triggering its price increase and supply shortage; • Sensitive to ambient environment (e.g., CO_2 and H_2O); • Low thermal stability (arouse safety concerns).	[42-45]

Improvement strategies for cation-disordered rock-salt cathodes

As an emerging group of high-power cathodes, the crystal configuration of the CDRS cathode materials, the mechanism of Li^+ insertion/extraction, and the fine-structure variation effects on the electrochemical performance have been intensely studied, as aforementioned above. For this series of materials, researchers focus on not only designing and regulating new hetero-structures but also modifying and optimizing existing CDRS systems. In this section, mostly applied optimization strategies are reviewed and discussed, which can be divided into three categories: morphology control, fluorine anion (F^-)-doping, and surface modification. **Morphology control**

Particles' size and morphology are critical influencing factors of cathode materials for LIBs. Commercial cathodes are mainly spherical powders within tens of micrometres, commonly fabricated via solid-state synthesis followed by large-scale mechanical ball milling and high-temperature post-calcination [46]. Although this process facilitates mass production, the high-temperature thermal treatment inevitably induces surface Li losses due to the relatively low decomposition temperatures of those usually used Li sources, which is detrimental for CDRS cathodes maintaining excess Li content. In addition, particle agglomerations during post-treatment further deteriorate the Li^+ diffusion rate in the rock-salt structures by lengthening the migration distance from the internal of cathode particle to the cathode-electrolyte interface (CEI). Various methods have been reported in these cases to adjust the morphology and particle size during synthesising CDRS oxides to enhance the electrochemical properties.

Recently, Zhang et al. studied the particle size-dependent effects on electrochemical redox kinetics and charge distributions taking $Li_{1.3}Mn_{0.4}Nb_{0.3}O_2$ (LMNO) as an example [47]. With different post-ball milling durations, the as-synthesized LMNO cathode particle sizes dropped from ~7 µm (0 h bill milling) to ~ 660 nm (18 h bill milling). The SEM images of the cathode powders with different milling times are illustrated in **Figure 2(a).** Accordingly, the initial specific discharge capacities dramatically increased from only ~10 mAh/g for pristine LMNO to 248 mAh/g after 18 h ball milling. **Figure 2(b)** shows the charge-discharge curves for each sample at a current rate of 20 mA/g. It can be seen that the LMNO cathode, after 18 h ball milling with the smallest particle size, maintained the highest specific energy after 20 cycles. The improved output should be attributed to the decreased particle size magnifying the specific area of cathode materials, leading to more abundant contact with electrolyte accelerating Li^+ exchange at CEI. Furthermore, the smaller volume of the cathode powders also shortens the Li^+ migration pathway, promoting the electrochemical kinetics of CRDS cathodes [48]. Chen et al. and Tarascon et al. investigated the electrochemical properties of single crystal (SC) and polycrystalline (PC) $Li_{1.3}Mn_{0.4}Ta_{0.3}O_2$ (LMTO), respectively, in 2019. Spherical shape SC-LTMO with a uniform size of ~5 µm was prepared by a molten-salt procedure [23], while Tarascon et al. obtained PC-LMTO from a classical solid-state process [24]. Comparing **Figure 2(c) and (d)**, the SC-LMTO with a smaller particle diameter could deliver a higher initial discharge capacity of ~250 mAh/g even cut at a higher voltage (1.5 V). However, the PC-LMTO only contributed ~180 mAh/g discharge capacity in the first cycle with the same current rate. Interestingly, when under a higher operation temperature, the specific capacities of PC-LMTO pronounced increase to ~270 mAh/g. Meng et al. also experimentally studied the morphology differences altering the electrochemical performances of CDRS oxides ($Li_{1.3}TM_{0.4}Nb_{0.3}O_2$; TM = Fe, Mn) by varying synthesis conditions. The nanoscale precursors were treated under a relatively low temperature with released particle aggregation, indicating enhanced cyclic reversibility (**Figure 2(e)**) [21]. They also proposed that CDRS cathodes share a similar issue with commercialized Ni-rich layered cathodes in that the initial discharge capacity would be

reduced under long-term air-expose caused by surface sensitivity to H_2O and CO_2 A recovery solution was provided, that is, thermal treatment at 500°C. Based on above discussion, we can conclude that the preparation process of CDRS materials is critical for optimizing the electrochemical performances because it greatly influences the morphology and size of cathodes, which further determines the redox kinetics of a LIB.

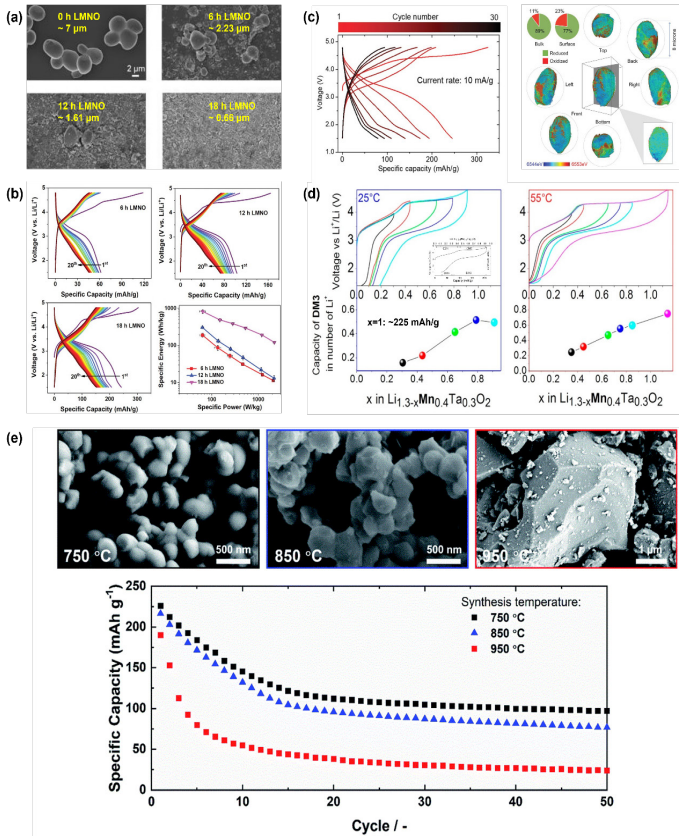

Figure 2: **(a)** SEM images of LMNO materials processed with different ball-mill time. **(b)** Electrochemical performance of the LMNO cells Voltage profiles at 20 mA/g, and the Ragone plots of different LMNO materials. Used with permission from ref.[47] © 2022 John Wiley and Sons. **(c)** Left: voltage profiles of SC-LMTO half-cell at 10 mA/g. Right: 3D distribution of the local edge energy over the Mn K-edge of an arbitrarily selected PC-LMTO particle that was exposed to NO_2BF_4 in an oxidant/oxide molar ratio of 0.5. Used with permission from ref.[23] © 2019 John Wiley and Sons. **(d)** 25 and 55 °C first galvanostatic cycles, respectively, made at different SOCs together with the discharge capacity, in number of Li, of DM3 (>3 V) in the bottom panel. Used with permission from ref. [24] © 2019 American Chemical Society. **(e)** Top: SEM images, and bottom: cycling stability of $Li_{1.3}Fe_{0.4}Nb_{0.3}O_2$ synthesized at a temperature of 750 °C (black), 850 °C (blue), and 950 °C (red). Used with permission from ref.[21] © 2021 Royal Society of Chemistry.

Fluorine anion-doping

Alteration of elemental composition and proportion of active materials is one of the most utilized strategies to adjust the electrochemical properties of electrode materials by modifying their crystal and electronic structures. For CDRS-class cathodes, incorporating high-valent TM with d^0 orbits and fluoride anion-doping in the oxygen sites are two commonly employed approaches to improve performance [49]. Apart from in-depth researched cationic dopants presented above, anion-doping, especially with F^- (1.33 Å), indicated promising merits because it could enlarge the sublattice to provide unobstructed space for the excess Li^+ diffusion, which also compensates the charge in the CDRS structure. Additionally, the higher electronegativity of the substituted F could reinforce the TM redox process more

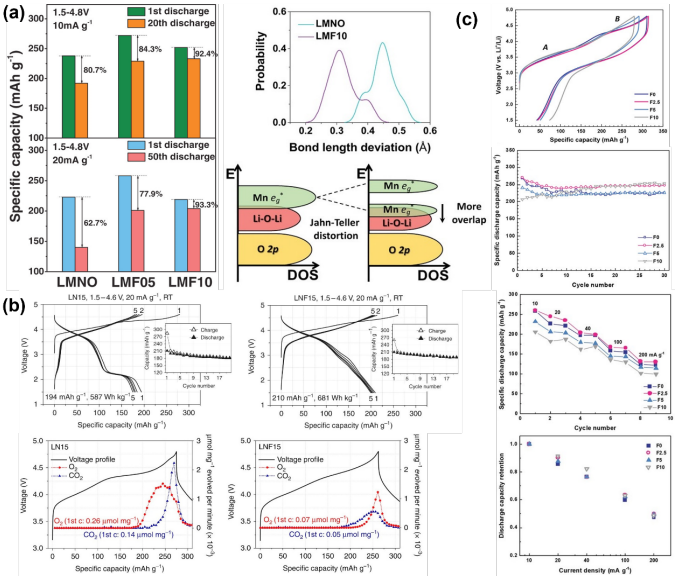

Figure 3: **(a)** Left: comparison of discharge capacities of LMNO, LMF05, and LMF10. Right: Distribution of calculated Mn-O/F bond-length deviations in LMNO and LMF10, and proposed structural connection between Jahn–Teller distortion and orbital energy levels. Used with permission from ref. [52] © 2018 John Wiley and Sons. **(b)** Top: voltage profiles of LN15 and LNF15 cycled between 1.5 and 4.6 V at 20 mA/g. The insets show the capacity retention of the materials over the first 20 cycles. Bottom; Differential electrochemical mass spectrometry (DEMS) of LN15 and LNF15. Used with permission from ref. [54] © 2017 Springer Nature. **(c)** Electrochemical performances of half-cells with different F doping levels. Top: voltage profiles during the first cycle. Upper middle: specific discharge capacity of F0, F2.5, F5, and F10 cathodes during the first 30 cycles. Lower middle: rate capability of as-prepared cathodes. Bottom: discharge capacity retention as a function of current densities. Used with permission from ref. [55] © 2020 John Wiley and Sons.

than TM-O bonds during cycling, contributing to extended reversible electrochemical reactions [50].

In 2017, Richard et al. initially verified that F doping into Mn-based cathodes is more favorable through DFT simulation, particularly with Li-rich and local TM deficiency environments [51]. Afterwards, Lun et al. successfully obtained a series of F-incorporated CDRS structures: $Li_{1.2}Mn^{3+}_{0.6+0.5x}Nb^{5+}_{0.2-0.5x}O_{2-x}F_x$ ($0 \le x \le 0.4$) [52]. The enhanced cyclability after F incorporation can be attributed to the significantly alleviated oxygen loss during cycling and decreased Jahn–Teller distortion originating from Mn^{3+}. In addition, They claimed that the 10% fluorination rearranges the energy levels of Mn and O in their orbital positions, as shown in **Figure 3(a)**. F^- breaks the symmetry of the electronic environment around Mn^{3+} may be responsible for the overall redox capacity improvement [53]. Lee et al. also comparative studied electrochemical performances between $Li_{1.15}Ni_{0.375}Ti_{0.375}Mo_{0.1}O_2$ (LN15) and $Li_{1.15}Ni_{0.45}Ti_{0.3}Mo_{0.1}O_{1.85}F_{0.15}$ (LNF15) [54]. Their results indicated that F could be not only facilely substituted into the bulk of CDRS oxides but also amplified the Ni redox activity during cycling. Their analysis confirmed that mitigated oxygen dissipation from the CRDS framework by F-doping significantly increases the practical energy density (from LN15 with 587 Wh/kg to LNF15 with 681 Wh/kg) (**Figure 3(b)**). LNF15 with a lower average anion valence due to charge compensation resulting in a lower polarization at reasonable operating voltages and exhibits a much higher rate capability than the pure LN15. Subsequently, Ahn et al. systematically explored the impact of the F-doping ratio on the electrochemical performance of $Li_{1.2}Mn_{0.6}Nb_{0.2}O_2$ [55]. It can be found from **Figure 3(c)** that

with the increase of F content, the initial discharge capacity was decreased correspondingly. However, the $Li_{1.2}Mn_{0.6}Nb_{0.2}O_{2-x}F_x$ exhibited better cyclic stability than the pristine one. The authors suggested that the F content increase lowers the anionic redox contribution ($O^{2-}/O^{(2-x)-}$) to the capacity while increasing the cationic redox activities, resulting in more reversible electrochemical properties for CDRS cathodes. It is also worth noting that rate capability increased with an appropriate amount of F substitution (2.5 at.%), possibly because of enhanced ionic and electronic conductivities.

1. In summary, the positive effects of F integration into CDRS systems can be concluded as follows: The bonding strength of Li-F higher than Li-O maximizes the Li content around F, stabilizing the Li-excess CDRS structure.

2. Irreversible anionic redox (oxygen release) during the initial cycle could be inhibited, increasing TM-based capacity contributions.

Local structure connections (such as short-range ordering) may be rearranged with F substitutions, promoting Li percolation in the rock-salt structure.

Surface modifications

Surface modification strategy has been commonly utilized on commercial cathode materials for years because coated cathode surface prevents direct contact with the organic electrolyte, avoiding parasitic reactions. Meanwhile, coating materials also locally reduce the acidity from the electrolyte at the CEI, which could suppress electrolyte degradation. In addition, employing high electrical conductive materials helps lower the internal resistance, facilitating the electrons and Li^+ transportations [56]. Considering oxygen anions are relatively active in CDRS oxides compared to other cathode materials, surface modification is an ideal way to improve and stabilize their cycling performance.

As mentioned above, CDRS cathodes usually possess high electrical resistance and fast capacity fading during cycles. In this regard, carbon-based coating materials are quite fit for CDRS oxides because of their high electronic conductivity, excellent stability, and low cost [57]. Shen et al. originated a $Li_{1.24}Fe_{0.38}Ti_{0.38}O_2$ (LFT) CDRS cathode coated with carbon nanotubes (CNTs) composited conductive networks, which indicates higher charge transfer and more sufficient Li diffusion rates [58]. The CNT surface-modified CDRS oxide showed a significantly enhanced rate performance. It can be observed from **Figure 4(a)** that the pristine LFT left only 36 mAh/g of discharge capacity after 200 cycles at a 300 mA/g current rate. After CNT coating, the reversible specific capacity drastically increased to 108 mAh/g at the same conditions. In the meantime, the long-term cycling (up to 500 cycles) of CNT/LFT cathode under 3000 mA/g reveals a negligible degradation.

The oxide-based coating could effectively suppress the side reactions between the cathode and electrolyte, thereby extending the cyclic stability of LIBs [59]. Huang et al. employed the atomic layer deposition (ALD) technique constructing a thin Al_2O_3 layer (less than 5 nm) onto CDRS $Li_{1.2}Ti_{0.4}Mn_{0.4}O_2$, intending to modify its electrochemical performances [60]. Their results turned out that with a proper thickness of Al_2O_3 coating (24 ALD cycles), the discharge capacity of LTMO/24Al_2O_3 increased from 228.1 to 266.7 mAh/g after 15 charge-discharge cycles at 10 mA/g with a capacity retention raising of 11.2% (from 79.7 to 90.9%), as illustrated in **Figure 4(b)**. The improved cycling stability of the Al_2O_3-coated sample is mainly due to the reduced undesirable side reactions, which alleviates the polarization during cycling. Furthermore, an artificially built oxide layer mitigates the charge transfer resistance from the spontaneously generated CEI, leading to improved electrochemical performance for CDRS cathode materials. Fichtner et al. investigated the electrochemical properties of $Li_{1.2}Ni_{1/3}Ti_{1/3}Mo_{2/15}O_2$ (LNTM) with or without $LiNbO_3$ (LNO) surface modification [29]. They have suggested that $LiNbO_3$ serve as not only a passivation layer to alleviate side reactions. At the same time, the Nb in the coating material would permeate into the LNTM cathode surface from the LNO-LNTM interface to establish a Li-Ni-Ti-Mo-Nb solid solution with Nb-rich regions under high-temperature thermal treatment. Compared to the pristine LNTM cathode manifesting substantial capacity decay at a high delithiation state due to irreversible oxygen release, dual modified (Nb doping/surface coating) LNTM cathode demonstrated enhanced discharge voltage and cyclic stability by reduction of impedance and polarization, respectively (**Figure 4(c)**). Their outcomes also confirm the necessity of using small-size materials for achieving high specific capacities in CDRS cathodes, which is well-agreed with the observations in section 3.1.

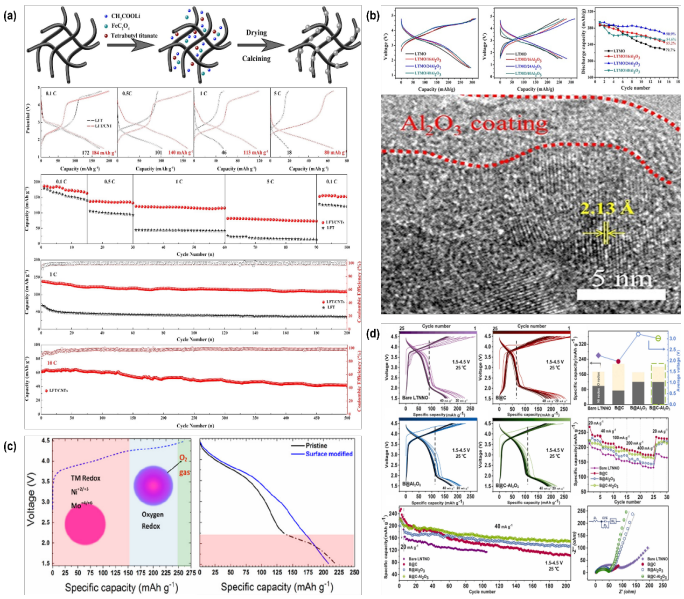

Figure 4: (a) From top to bottom: schematic fabrication process of LFT/CNT; voltage profiles and rate capabilities of the LFT and LFT/CNT cathodes at various rates (0.1 C to 5 C); cycling performance and coulombic efficiency of the LFT and LFT/CNT cathodes at current rates of 1 C and 10 C (1 C = 300 mA/g). Used with permission from ref. [58] © 2021 Springer Nature. **(b)** Top left and middle: 1st and 10th charge-discharge curves. Top right: cyclic performance of as-prepared cathodes. Bottom: HRTEM images LTMO/24Al_2O_3. Used with permission from ref. [60] © 2019 Huang, Wang, Gong, He and Wang. **(c)** Voltage profiles pristine LNTM and LNO-coated LNTM cathodes. Used with permission from ref.[29] © 2019 American Chemical Society. **(d)** Electrochemical properties of LTNNO, LTNNO@C, LTNNO@Al_2O_3, and LTNNO@C-Al_2O_3. Used with permis*sion from ref. [7] © 2022 Elsevier.*

Very recently, Yu et al. attempted carbon/Al_2O_3 double coating on a Ni-based CDRS oxide: $Li_{1.2}Ti_{0.3}Ni_{0.3}Nb_{0.2}O_2$ (LTNNO) [7]. Among all control groups, carbon and Al_2O_3 co-coated cathodes presented improved long-term redox stability (delivered a reversible capacity of more than 149 mAh/g after 200 cycles at 40 mA/g with a capacity retention of 76.1%). It is also corroborated that carbon coating promotes capacity by increasing the conductivity of the CDRS compositions. After the sole carbon coating, they found that a new generation of peroxo-like species boosts anionic capacity contributions. Additionally, Al_2O_3

coating accompanied by partially smaller radius Al^{3+} doping on Ti sites improved the cycling stability of the CDRS cathodes because of the protective effect on parasitic reactions and shortening the band overlap between Ni and O, activating Ni redox couples and stabilizing O sublattice.

In short, we conclude that surface modifications promise further improvement of the rate capability and cycling performance of Li-excess Co-free CDRS cathode materials.

Conclusions and Prospects

As electronics have become indispensable in human life in recent years, the demand for high-performance LIBs is significantly increasing. CDRS-based cathode materials diversify the battery landscape and help alleviate the over-reliance on toxic Co, leading to a promising future for the energy storage market. However, most CDRS cathodes were restricted by low electrical conductivity, slow Li^+ diffusion, and unfavourable electrolyte interactions. Researchers have put in years of effort to overcome these challenges through different methods. Hence, after a systematic review of nearly a decade of literature in this area, we categorize these improvement strategies for CDRS cathode materials into three classes: morphology control and size minimization, elemental doping, and surface modification. Except for the improvement mechanisms already expressed above, several questions and proposals for the next-generation CRDS cathodes are provided below for continuing investigation:

1. Without a doubt, downsizing CDRS particles to the nanoscale benefits achieving high power density since it reduces the Li^+ diffusion length and the migration barrier. However, small particle size will also enhance the anionic redox activity, triggering irreversible oxygen loss. Therefore, a passivation layer may inhibit this effect worth further analyzing.

2. In CDRS oxides, unhybridized O 2p orbitals arouse oxygen loss at a high delithiation state. Thus, F doping at the oxygen sites can be used to increase the TM-based redox capacities. However, the doping amount in diverse CDRS systems is blurred.

3. Although positive impacts have been claimed after the surface modifications on the CDRS cathodes, functionalities and mechanisms still need to be better understood. Also, optimizing the coating process to achieve uniform coating is a critical technical problem that needs to be solved.

4. As the research for CDRS cathodes is still in the early stages, continuing to find CDRS materials with low cost, controllable production processes and excellent performance, as well as an in-depth discussion of related mechanisms, will still be the research focus in the future.

5. Comprehensive analysis of the modification strategies with various doping elements and coating materials, such as polymers with excellent conductivity and electrochemical activity, should be paid more attention to modifying CDRS cathode materials. The CDRS cathodes may also be integrated into the emerged lithium-sulphur (Li-S) or lithium-air/oxygen (Li-air) systems to explore more possibilities.

Disclosure statement

The authors declare no competing financial interest.

Acknowledgment

Peiyuan Guan would like to thank the financial support from Research Training Program (RTP) funded by the Department of Education, Australian Government.

Highlights

- Recent development of cation-disordered rock-salt cathode materials in lithium-ion batteries has been systematically reviewed.
- State-of-art research progress focusing on the improvement strategies and corresponding mechanisms for cation-disordered rock-salt cathodes have been summarized.
- Prospect for optimizing cation-disordered rock-salt cathode materials are discussed.

References

1. Manthiram A. A reflection on lithium-ion battery cathode chemistry. Nat Commun. 2020; 11: 1550.
2. Guan P, Zhou L, Yu Z, Sun Y, Liu Y, et al. Journal of Energy Chemistry. 2020; 43: 220-235.
3. Hu B, Geng FS, Shen M, Zhao C, Qiu Q, et al. Power Sources. 2021; 516.
4. Li JL, Fleetwood J, Hawley WB, Kays W. Chem Rev. 2022; 122: 903-956.
5. Purwanto A, Yudha CS, Ubaidillah U, Widiyandari H, Ogi T, et al. Materials Research Express. 2018; 5.
6. Lee S, Manthiram A. ACS Energy Letters. 2022; 7: 3058-3063.
7. Yu Z, Huang H, Liu Y, Qu X, Zhou Y, et al. Nano Energy. 2022; 96: 107071.
8. Zeitschrift für Kristallographie - Crystalline Materials.1990; 190: 161-169.
9. Lee J, Urban A, Li X, Su D, Hautier G, et al. Science. 2014; 343: 519-522.
10. Lee J, Seo DH, Balasubramanian M, Twu N, Li X, et al. Energy Environ Sci. 2015; 8: 3255-3265.
11. Yabuuchi N. Current Opinion in Electrochemistry. 2022; 34: 100978.
12. Wang MX, Chen XC, Yao HR, Lin GG, Lee J, et al. Energy Environ Mater. 2022; 5: 1139-1154.
13. Kitajou A, Tanaka K, Miki H, Koga H, Okajima T, et al. Electrochem. 2016; 84: 597-600.
14. Yabuuchi N, Nakayama M, Takeuchi M, Komaba S, Hashimoto Y, et al. Nat Commun. 2016; 7: 13814.
15. Ji H, Urban A, Kitchaev DA, Kwon DH, Artrith N, et al. Nat Commun. 2019; 10: 592.
16. Lee J, Wang C, Malik R, Dong Y, Huang Y, et al. Advanced Energy Materials.2021; 11: 2100204.
17. Wang R, Huang B, Qu Z, Gong Y, He B, et al. Solid State Ionics. 2019; 339: 114999
18. Chen, Kan WH, Chen G. Advanced Energy Materials 9(31) (2019) 1901255
19. Kwon DH, Lee J, Artrith N, Kim H, Wu LJ, et al. Cell Rep Phys Sci. 2020; 1.

20. Kan WH, Chen D, Papp JK, Shukla AK, Huq A, et al. Chem Mater. 2018; 30: 1655-1666.

21. Chung H, Lebens-Higgins Z, Sayahpour B, Mejia C, Grenier A, et al. J Mater Chem A. 2021; 9: 1720-1732.

22. Yabuuchi N, Takeuchi M, Nakayama M, Shiiba H, Ogawa M, et al, Proc Natl Acad Sci USA. 2015; 112: 7650-7655.

23. Kan WH, Wei C, Chen D, Bo T, Wang BT, et al. Adv Funct Mater. 2019; 29: 1808294.

24. Jacquet Q, Iadecola A, Saubanère M, Li H, Berg EJ, et al. J Am Chem Soc. 2019; 141: 11452-11464.

25. Zhao W, Yamaguchi K, Sato T, Yabuuchi N. J Electrochem Soc. 2018; 165: A1357.

26. Liu Y, Zheng S, Wan H, Dou A, Chu D. J Alloys Compd. 2017; 728: 659-668.

27. Zheng S, Liu D, Tao L, Fan X, Liu K, et al. J Alloys Compd. 2019; 773: 1-10.

28. Lee J, Seo DH, Balasubramanian M, Twu N, Li X, et al. Energy Environ Sci. 2015; 8: 3255-3265.

29. Cambaz MA, Vinayan BP, Geßwein A, Schiele A, Sarapulova T, et al. Chem Mater. 2019; 31: 4330-4340.

30. Yu Z, Qu X, Dou A, Su M, Liu Y, Wu F. ACS Appl Mater Interfaces. 2019; 11: 35777-35787.

31. Lin H, Moreno B, Kucuk K, Zhang S, Aryal S, et al. IJER. 2021; 45: 3966-3978.

32. Wu Z, Luo Q, Lin L, Yang W, Zou H, Yu H, Chen S. IJER. 2021; 45: 3966-3978.

33. Twu N, Li X, Urban A, Balasubramanian M, Lee J, et al. Nano Lett. 2015; 15: 596-602.

34. Wang X, Huang W, Tao S, Xie H, Wu C, et al. Power Sources. 2017; 359: 270-276.

35. Li X, Qiao Y, Guo S, Jiang K, Ishida M, et al. Adv Mater. 2019; 31: 1807825.

36. Nakajima M, Yabuuchi N. Chem Mater. 2017; 29: 6927-6935.

37. Yabuuchi N, Takeuchi M, Komaba S, Ichikawa S, Ozaki T, et al. Chem Commun. 2016; 52: 2051-2054.

38. Hoshino S, Glushenkov AM, Ichikawa S, Ozaki T, Inamasu T, et al. ACS Energy Letters. 2017; 2: 733-738.

39. Urban A, Abdellahi A, Dacek S, Artrith N, Ceder G. Phys Rev Lett. 2017; 119: 176402.

40. Clément RJ, Lun Z, Ceder G. Energy Environ Sci. 2020; 13: 345-373.

41. Muralidharan N, Self EC, Dixit M, Du ZJ, Essehli R, et al. Advanced Energy Materials. 2022; 12.

42. Guan PY, Zhu YZ, Li MY, Zeng TY, Li XW, et al. Colloid Interface Sci. 2022; 628: 407-418.

43. Zhang R, Wang CY, Zou PC, Lin RQ, Ma L, et al. Nature. 2022; 610.

44. Park NY, Park GT, Kim SB, Jung W, Park BC, Sun YK, Acs Energy Letters. 2022.

45. Li H, Fong R, Woo M, Ahmed H, Seo DH, et al. Joule. 2022; 6: 53-91.

46. WANG Li HX, GAO Jian, LI Jianjun, JIANG Changyin, Energy Storage Science and Technology. 2018; 7: 888-896.

47. Zhang Y, Hu A, Liu J, Xu Z, Mu L, et al. Adv Funct Mater. 2022; 32: 2110502.

48. Choi H, Schuer AR, Moon H, Kuenzel M, Passerini S. Electrochim. Acta. 2022; 430.

49. Chen D, Ahn J, Chen G. ACS Energy Letters. 2021; 6: 1358-1376.

50. Shirazi Moghadam Y, Dinda S, El Kharbachi A, Melinte G, Kübel C, et al. Chem Mater. 2022; 34: 2268-2281.

51. Richards WD, Dacek ST, Kitchaev DA, Ceder G. Advanced Energy Materials. 2018; 8: 1701533.

52. Lun Z, Ouyang B, Kitchaev DA, Clément RJ, Papp JK, et al. Advanced Energy Materials. 2019; 9: 1802959.

53. Seo DH, Lee J, Urban A, Malik R, Kang S, et al. Nat Chem. 2016; 8: 692-697.

54. Lee J, Papp JK, Clément RJ, Sallis S, Kwon DH, et al. Nat Commun. 2017; 8: 981.

55. Ahn J, Chen D, Chen G. Advanced Energy Materials. 2020; 10: 2001671.

56. Sun YD, Guan PY, Liu YJ, Xu HL, Li SA, et al. Crit Rev Solid State Mater Sci. 2019; 44: 265-282,

57. Zhou K, Zheng S, Liu H, Zhang C, Gao H, et al. ACS Appl Mater Interfaces. 2019; 11: 45674-45682.

58. Shen Y, Yang Y, Li J, Yang M, Zhao X, et al. J Electron Mater. 2021; 50: 5029-5036.

59. Xu M, Chen Z, Zhu H, Yan X, Li L, et al. J Mater Chem A. 2015; 3: 13933-13945.

60. Huang BJ, Wang R, Gong YS, He BB, Wang HW. Front Chem. 2019; 7.